



# Enhanced Photocatalytic Activity for H<sub>2</sub> Evolution under Irradiation of UV–Vis Light by Au-Modified Nitrogen-Doped TiO<sub>2</sub>

Weirong Zhao\*, Zhuyu Ai, Jiusong Dai, Meng Zhang

Department of Environmental Engineering, Zhejiang University, Hangzhou, China

## Abstract

**Background Purpose:** Photocatalytic water splitting for hydrogen evolution is a potential way to solve many energy and environmental issues. Developing visible-light-active photocatalysts to efficiently utilize sunlight and finding proper ways to improve photocatalytic activity for H<sub>2</sub> evolution have always been hot topics for research. This study attempts to expand the use of sunlight and to enhance the photocatalytic activity of TiO<sub>2</sub> by N doping and Au loading.

**Methods:** Au/N-doped TiO<sub>2</sub> photocatalysts were synthesized and successfully used for photocatalytic water splitting for H<sub>2</sub> evolution under irradiation of UV and UV–vis light, respectively. The samples were characterized using X-ray diffraction (XRD), transmission electron microscopy (TEM), X-ray photoelectron spectroscopy (XPS), UV–vis diffuse reflectance spectroscopy (DRS), photoluminescence spectroscopy (PL), and photoelectrochemical characterizations.

**Results:** DRS displayed an extension of light absorption into the visible region by doping of N and depositing with Au, respectively. PL analysis indicated electron-hole recombination due to N doping and an efficient inhibition of electron-hole recombination due to the loaded Au particles. Under the irradiation of UV light, the photocatalytic hydrogen production rate of the as-synthesized samples followed the order Au/TiO<sub>2</sub> > Au/N-doped TiO<sub>2</sub> > TiO<sub>2</sub> > N-doped TiO<sub>2</sub>. While under irradiation of UV–vis light, the N-TiO<sub>2</sub> and Au/N-TiO<sub>2</sub> samples show higher H<sub>2</sub> evolution than their corresponding nitrogen-free samples (TiO<sub>2</sub> and Au/TiO<sub>2</sub>). This inconsistent result could be attributed to the doping of N and the surface plasmonic resonance (SPR) effect of Au particles extending the visible light absorption. The photoelectrochemical characterizations further indicated the enhancement of the visible light response of Au/N-doped TiO<sub>2</sub>.

**Conclusion:** Comparative studies have shown that a combination of nitrogen doping and Au loading enhanced the visible light response of TiO<sub>2</sub> and increased the utilization of solar energy, greatly boosting the photocatalytic activity for hydrogen production under UV–vis light.

**Citation:** Zhao W, Ai Z, Dai J, Zhang M (2014) Enhanced Photocatalytic Activity for H<sub>2</sub> Evolution under Irradiation of UV–Vis Light by Au-Modified Nitrogen-Doped TiO<sub>2</sub>. PLoS ONE 9(8): e103671. doi:10.1371/journal.pone.0103671

**Editor:** Elena A. Rozhkova, Argonne National Laboratory, United States of America

**Received:** May 18, 2014; **Accepted:** June 30, 2014; **Published:** August 4, 2014

**Copyright:** © 2014 Zhao et al. This is an open-access article distributed under the terms of the Creative Commons Attribution License, which permits unrestricted use, distribution, and reproduction in any medium, provided the original author and source are credited.

**Data Availability:** The authors confirm that all data underlying the findings are fully available without restriction. All relevant data are within the paper and its Supporting Information files.

**Funding:** This work has been partially supported by the National Nature Science Foundation of China (Grant nos. 51178412 and 51278456, <http://www.nsf.gov.cn>) and the National Key Technologies R&D Program (Grant no. 2013BAC16B01, <http://www.most.gov.cn>). The funders had no role in study design, data collection and analysis, decision to publish, or preparation of the manuscript.

**Competing Interests:** The authors have declared that no competing interests exist.

\* Email: [weirong@mail.hz.zj.cn](mailto:weirong@mail.hz.zj.cn)

## Introduction

Energy and environmental issues have become the focus of world attention. Developing clean and renewable energy is a crucial step in solving these issues. The conversion of solar energy to hydrogen via photocatalytic water splitting presents a promising alternative for a renewable, clean and economical process [1–3]. Exploiting visible-light-active photocatalysts for the efficient utilization of sunlight and finding proper ways to improve photocatalytic activity for H<sub>2</sub> evolution are still the major challenges preventing photocatalytic water splitting, therefore, receive a lot of attention from researchers.

N-doped TiO<sub>2</sub> has been widely studied because of its ability to extend the light absorption of TiO<sub>2</sub> into the visible region [4,5]. It

was reported that the localized states introduced via nitrogen doping and simultaneously induced oxygen vacancies were responsible for the visible light photoactivity [6]. However, these impurity levels may enhance the recombination rate of photo-generated electrons and holes, thus decreasing the photocatalytic activity [7,8]. As one of the most promising methods to improve photocatalytic efficiency, loading of noble metals, such as Au, Ag, or Pt, has also been extensively studied [9–12]. These noble metals can effectively promote the transfer of photoinduced electrons due to the formation of a Schottky barrier at the interface between the metal and the semiconductor, thereby reducing the recombination of photogenerated charge carriers, resulting in an enhancement of the photocatalytic activity. Meanwhile, Au-loaded samples have attracted broad attention [13] because it is a plasmonic metal with

a surface plasmonic resonance (SPR) effect that supposedly has the ability to increase visible light photocatalytic efficiency, e.g., Au-loaded TiO<sub>2</sub> [14] and Au-loaded ZnO [15].

Based on the specific features of nitrogen doping and Au loading, it is possible to compensate for the deficiencies in the N doping by Au loading, thereby expanding the utilization of solar energy and boosting the photocatalytic activity for hydrogen evolution. Sanz et al. [16] reported that Au adsorption on N-doped TiO<sub>2</sub> (Au/N-TiO<sub>2</sub>) surfaces led to a higher stabilization of N species and a synergic effect between implanted N and deposited Au atoms. The Au/Ti<sub>x</sub>N<sub>y</sub>O<sub>2-y</sub> system was able to catalyze hydrogen evolution via the water-gas shift reaction at elevated temperatures (575–625 K). Tian et al. [17] adopted a simple wet-chemical method to prepare Au/N-TiO<sub>2</sub> photocatalysts, which exhibited much higher visible-light photocatalytic activity than N-doped or Au-loaded TiO<sub>2</sub>. Wu et al. [18] reported that Au/N-TiO<sub>2</sub> exhibited a much higher photocatalytic activity in the degradation of methyl orange compared to N-TiO<sub>2</sub> due to the appropriate sizes of Au particles and the synergic effect between the N dopant and the Au particles. Despite the current progress, the exploration of Au/N-TiO<sub>2</sub> photocatalysts, especially for their application in photocatalytic water splitting for H<sub>2</sub> generation, is still very necessary.

In the present work, the photocatalytic water splitting for H<sub>2</sub> generation by TiO<sub>2</sub>, N-doped TiO<sub>2</sub>, Au-loaded TiO<sub>2</sub> and Au-modified N-doped TiO<sub>2</sub> was compared under irradiation of UV and UV-vis light. The photocatalytic mechanism of Au/N-TiO<sub>2</sub> was further investigated using DRS, PL, and photoelectrochemical characterization.

## Experimental Section

### Chemicals and sample preparation

P25 (Degussa, Germany) was used in the preparation of TiO<sub>2</sub> and N-doped TiO<sub>2</sub>. Chloroauric acid tetrahydrate (AuCl<sub>3</sub>·HCl·4H<sub>2</sub>O), sodium hydroxide (NaOH), nitric acid (HNO<sub>3</sub>), ammonia solution (NH<sub>4</sub>OH), sodium sulfate anhydrous (Na<sub>2</sub>SO<sub>4</sub>), methanol (CH<sub>3</sub>OH), and ethanol (C<sub>2</sub>H<sub>6</sub>O) were all analytical grade and purchased from Sinopharm Chemical Reagent Co., Ltd, China. All chemicals were used as received without further purification.

N-doped TiO<sub>2</sub> was prepared using a typical hydrothermal method similar to our previous work [19]. A mixture of 1.5 g P25 powder and 70 ml of 10 M NaOH solution was heated at 150°C for 48 h in a Teflon-lined autoclave. After cooling, the precipitate was neutralized thoroughly by washing with a 0.1 M HNO<sub>3</sub> solution and distilled water. Then, the precipitate was aged in a 0.5 M HNO<sub>3</sub> solution and placed in a 0.5 M NH<sub>4</sub>OH solution for 24 h, respectively. The resulting powder was dried at 80°C for 8 h to obtain N-doped titanium nanotubes (NTNT). Yellow colored N-doped TiO<sub>2</sub> was finally obtained after being calcined at 400°C for 1 h in air and designated as N-TiO<sub>2</sub>. Titanium nanotubes (TNT) and TiO<sub>2</sub> samples for comparison were prepared in the same method as above without the steps of aging and ammonia impregnation.

The Au loading process was performed using a photoreduction method as described previously [20]. First, 0.3 g of N-TiO<sub>2</sub> or TiO<sub>2</sub> was dispersed into the mixture of 60 mL deionized water and 15 mL methanol, then a 628 μL solution of 10 mg/mL AuCl<sub>3</sub>·HCl·4H<sub>2</sub>O was added as the gold precursor (1 wt% or 0.41 at% Au loaded on the base material). The pH of the suspensions solution was adjusted to ca. 7.0 using 0.1 M NaOH, and the resulting mixture was dispersed by ultrasound for 15 min. The reaction system was magnetic stirred using a magnetic stirrer and

ventilated under a continuous flow of Ar gas to remove the oxygen from the reactor. Four UV lamps (4 W, 254 nm, Xuanfeng, China) were used to irradiate the slurry for 2 h with an irradiation intensity of ca. 8 mW/cm<sup>2</sup>. Then, the precipitate was filtered and washed with distilled water three times. Finally, the solid was dried at 60°C overnight under air to obtain Au-modified N-doped TiO<sub>2</sub> or Au-loaded TiO<sub>2</sub> and designated Au/N-TiO<sub>2</sub> or Au/TiO<sub>2</sub>, respectively.

### Material characterization

The crystal phases of the samples were analyzed by X-ray diffraction (XRD) patterns (X'Pert Pro, PANalytical, Holland) using Cu Kα radiation ( $\lambda = 1.5418 \text{ \AA}$ ) at 40 kV and 150 mA.

The morphology and nanostructure of samples were examined by a transmission electron microscopy (TEM, FEI, USA) and a high resolution TEM (HRTEM).

The surface properties of Au/N-TiO<sub>2</sub> were investigated using X-ray photoelectron spectroscopy (XPS, Thermo ESCALAB 250, USA). Al Kα radiation ( $h\nu = 1486.6 \text{ eV}$ ) was used as the X-ray source. All bonding energies were calibrated to the C 1s internal standard.

The light absorption properties of the samples were analyzed by UV-vis diffuse reflectance spectra (DRS) using a UV-vis spectrophotometer (TU-1901, Pgeneral, China) equipped with an integrating sphere assembly.

The photoluminescence spectra (PL) were measured with a Fluorolog-3-Tau spectrophotometer using a UV lamp of 254 nm as the excitation source.

The incident visible and UV light intensities were detected using a radiometer (FZ-A, Handy, China) and a UV light meter (ST-512, Sentry, China), respectively.

### Photoelectrochemical measurements

Photoelectrochemical measurements were performed using an electrochemical workstation (CH Instruments 650D, Shanghai, China) with a standard three-electrode quartz cell, as described in our previous work [21]. Two UV lamps (4 W, 254 nm, Xuanfeng, China) and a 300 W xenon (Xe) lamp (CEL-HXUV300, CeAulight, China) filtered with VisREF (350–780 nm) and UVIR-CUT400 (400–780 nm) were used as UV (ca. 2 mW/cm<sup>2</sup>) and visible light (ca. 20 mW/cm<sup>2</sup>) sources, respectively. A solution of 0.1 M Na<sub>2</sub>SO<sub>4</sub> and absolute ethanol with a volume ratio of 4:1 was used as electrolytes and degassed under nitrogen gas for 15 min prior to electrochemical measurements. Photocurrent densities vs. time curves were obtained at zero bias voltage irradiated with UV ( $\lambda = 254 \text{ nm}$ ) or visible light ( $\lambda > 400 \text{ nm}$ ) for 20 s. Electrochemical impedance spectroscopy (EIS) was obtained in the frequency range from 1 Hz to 1 MHz at an amplitude of 5 mV, and the applied bias voltage was set at open-circuit voltage.

### Photocatalytic activity

Photocatalytic hydrogen production experiments were performed in a top-irradiation jacketed quartz photoreactor in which the temperature was maintained using flowing water in the jacket around the reactor. In a typical reaction, 50 mg of the photocatalyst was dispersed by magnetic stirring in a 50 mL of 30% methanol/water aqueous solution. Before illumination, high-purity Ar gas was bubbled for 1 h to completely remove residual oxygen. A 300 W xenon (Xe) lamp (CEL-HXUV300, CeAulight, China) filtered with VisREF (350–780 nm) and three UV lamps (4 W, 254 nm, Xuanfeng, China) were used as the UV-vis and UV light sources, respectively. The resulting gas was periodically detected using a gas chromatograph (Fuli 9790, China) equipped

with a thermal conductivity detector at intervals of 1 h with Ar as the carrier gas.

## Results and Discussion

### Structure and morphology

Figure 1 shows the XRD patterns of P25, TNT, TiO<sub>2</sub>, N-TiO<sub>2</sub>, and Au/N-TiO<sub>2</sub>. It can be observed that pure P25 exhibits diffraction peaks at 25.26°, 37.78°, 48.00°, 53.79°, 55.02°, 62.63°, 68.79°, 70.38°, and 75.10° indexed to the (101), (004), (200), (105), (211), (204), (116), (220), and (215) crystal planes of anatase TiO<sub>2</sub> (JCPDS 21-1272), respectively. It also shows diffraction peaks at 27.39°, 36.02°, 41.22°, 56.61° and 64.01°, corresponding to the (110), (101), (111), (220), and (310) planes of rutile TiO<sub>2</sub> (JCPDS 21-1276), respectively. After hydrothermal treatment, the as-prepared TNT does not show peaks corresponding to anatase, rutile, brookite, or the mixtures of them. According to the literature [22], the crystal structure of TNT can be designated as a structural variant of H<sub>2</sub>Ti<sub>3</sub>O<sub>7</sub>. The XRD patterns of TiO<sub>2</sub>, N-TiO<sub>2</sub>, and Au/N-TiO<sub>2</sub> show the same peaks corresponding to anatase, indicating that H<sub>2</sub>Ti<sub>3</sub>O<sub>7</sub> completely converted to anatase TiO<sub>2</sub> during calcination. The results also demonstrate that the implanted nitrogen and deposited Au have almost no effect on the crystal orientations of TiO<sub>2</sub>. New peaks at 38.21°, 44.38°, and 77.56°, corresponding to (111), (200), and (311) planes of polycrystalline Au (JCPDS 04-0784), appear in the XRD pattern of Au/N-TiO<sub>2</sub>, confirming the existence of Au. These peaks are not particularly obvious, which could be attributed to the low concentration of Au.

TEM images of Au/N-TiO<sub>2</sub> are displayed in Figure 2a. After calcination, the Au/N-TiO<sub>2</sub> photocatalysts turn into nano-bulk,

and the Au particles attached onto the surface of N-TiO<sub>2</sub> are approximately 20–30 nm. The SAED pattern in the inset of Figure 2a shows rings that correspond to anatase TiO<sub>2</sub> (101), (004), and (200). Figure 2b shows a high-resolution TEM (HRTEM) image of a representative Au nanoparticle attached to N-TiO<sub>2</sub>; two distinct lattice spacings are observed, which match the interplanar spacings of anatase TiO<sub>2</sub> and Au, respectively. The measured distance between TiO<sub>2</sub> lattice planes is 0.360 nm, which corresponds to anatase TiO<sub>2</sub> (101), and the lattice fringes corresponding to the (111) plane of Au are 0.239 nm. The EDS spectrum of Au/N-TiO<sub>2</sub> indicates the presence of N and Au (Figure 2c).

### Surface analysis

XPS was used to determine the chemical state of Au/N-TiO<sub>2</sub> (Figure 3). Figure 3a shows the entire XPS survey of Au/N-TiO<sub>2</sub>. The presence of the C 1s peak located at a binding energy (BE) of 286.0 eV is attributed to the adhesive tape used in the XPS measurement. Figure 3b shows the high-resolution XPS spectra for the O 1s region of Au/N-TiO<sub>2</sub>. Three peaks at 529.6, 531.3, and 532.1 eV can be observed, indicating three different O state types. According to the literature [23,24], peaks centered at 529.6 and 531.3 eV can be assigned to oxygen in Ti–O–Ti and Ti–O–N bonds in the lattice, respectively. The third peak at 532.1 eV can be attributed to the Ti–O–H bonds resulting from chemisorbed water [25]. There are two types of N species in TiO<sub>2</sub> lattice, including interstitial N (Ni<sup>•</sup>) and substitutional N (Ns<sup>•</sup>). Ni<sup>•</sup> proved to be more favorable from the viewpoint of energy based on DFT calculations [26]. N 1s XPS spectra are shown in Figure 3c. After nitrogen doping, an N 1s peak with a core level BE of 399.7 eV is observed, as also reported in the literature [27,28]. The result

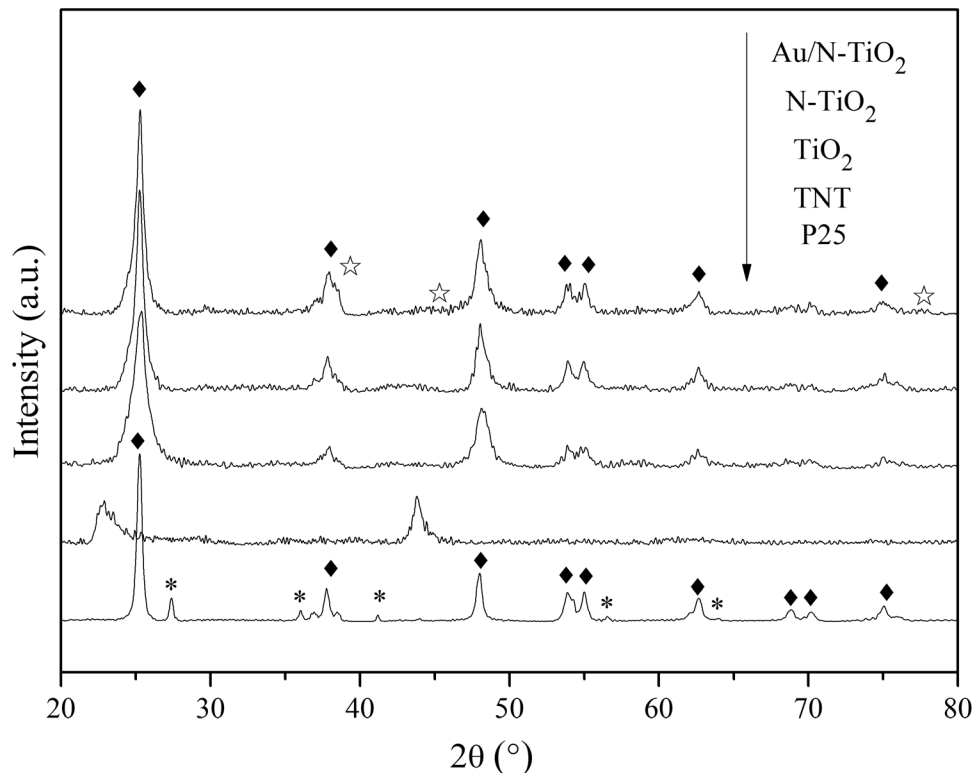


**Figure 1.** XRD patterns of P25, TNT, TiO<sub>2</sub>, N-TiO<sub>2</sub> and Au/N-TiO<sub>2</sub>. Asterisk, rhombus, and open star denote rutile, anatase, and Au, respectively.

doi:10.1371/journal.pone.0103671.g001

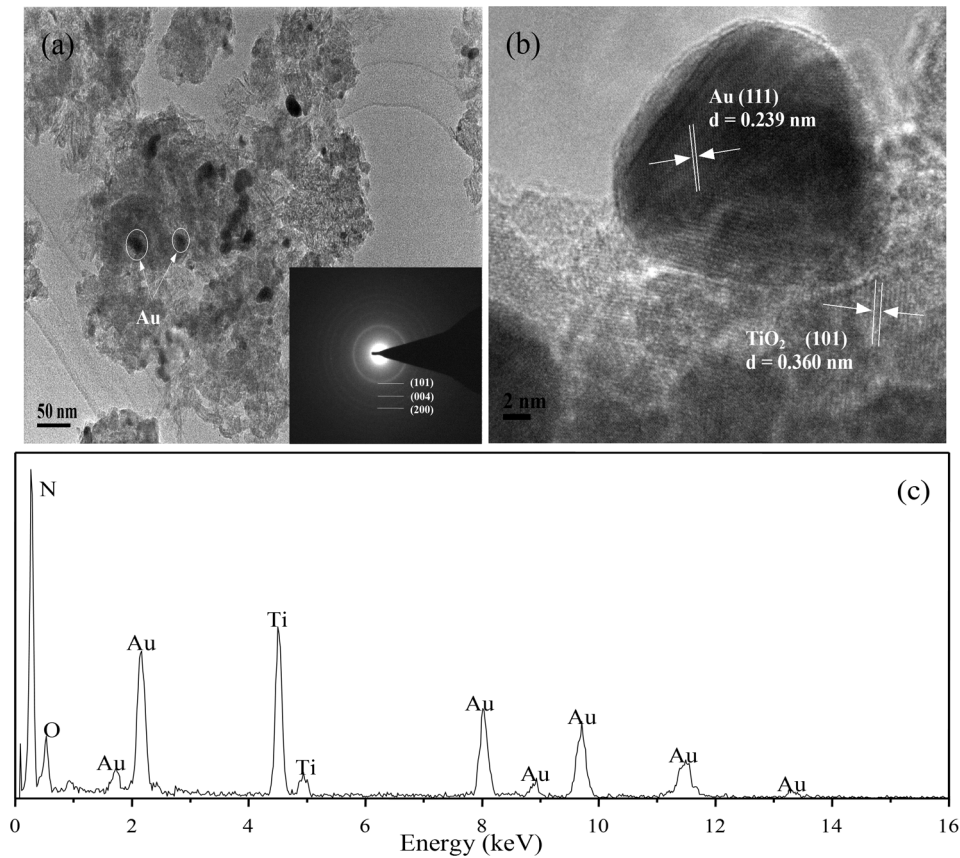


**Figure 2. (a) TEM image of as synthesized Au/N-TiO<sub>2</sub>, inset in the lower right corner is the SAED pattern of anatase TiO<sub>2</sub> and (b) HRTEM image and (c) EDX spectrum of Au/N-TiO<sub>2</sub>.**  
doi:10.1371/journal.pone.0103671.g002

proves that the doped N species are in interstitial positions bound directly to lattice oxygen, which is consistent with the theoretical calculations, and the linkages to nitrogen atoms may be in the state of Ti-O-N or Ti-N-O [29]. Figure 3d shows the XPS Au 4f spectra of the Au/N-TiO<sub>2</sub> samples. Double peaks for gold nanoparticles are found at 82.8 and 86.5 eV, corresponding to Au 4f<sub>7/2</sub> and Au 4f<sub>5/2</sub>, indicating a shift of the Au 4f peaks toward lower binding energies compared with the peaks located at 83.3 and 87.2 eV [30,31], respectively, which is most likely due to the intimate contact between the Au and the N-TiO<sub>2</sub> substrate, leading to a change in the electronic properties [18]. The amount of Au and N measured by XPS were 0.27 at% and 0.18 at%, respectively.

### Optical properties

Figure 4 shows the DRS of TiO<sub>2</sub>, Au/TiO<sub>2</sub>, N-TiO<sub>2</sub>, and Au/N-TiO<sub>2</sub>. It can be observed that the absorption spectrum of TiO<sub>2</sub> is cut off at 400 nm, while N-TiO<sub>2</sub> sample shows significant absorption in the visible region between 400 and 550 nm. It was reported that single-atom nitrogen impurities (including N<sup>+</sup> and N<sup>s\*</sup>) can form either diamagnetic (N<sub>b</sub><sup>-</sup>) or paramagnetic (N<sub>b</sub><sup>•</sup>) bulk centers, and both of them can give rise to localized states in the band gap of the oxide [32]. Under irradiation, a reversible electron transfer between charged diamagnetic N<sub>b</sub><sup>-</sup> and neutral paramagnetic N<sub>b</sub><sup>•</sup> can form, simultaneously resulting in the excitation of electrons into the conduction band; therefore, they play an essential role in the absorption of visible light [33]. Oxygen vacancies induced by nitrogen doping in TiO<sub>2</sub> can act as color

centers and can also contribute to the visible light absorption [8]. In addition, after loading with Au, another absorbance band at approximately 550 nm can be found and is attributed to the surface plasmonic resonance (SPR) effect of the Au nanoparticles [34,35]. Metal nanoparticles, such as Au, Cu, and Ag, are able to absorb and scatter photons in the visible region. When the particles are illuminated, the free conduction band electrons will oscillate under the force exerted by the electromagnetic field of the light, resulting in a strong-field enhancement of the local electromagnetic field and the appearance of plasmon absorption bands [36]. This near-field optical enhancement is hypothesized to increase the electron-hole pair generation rate and to enhance the photocatalytic activity accordingly [37,38].

PL emission spectra were used to measure the altered electronic properties of the as-prepared photocatalysts, including the immigration, transfer, and recombination processes of the charge carriers [39,40]. Figure 5 demonstrates the PL spectra of TiO<sub>2</sub>, Au/TiO<sub>2</sub>, N-TiO<sub>2</sub>, and Au/N-TiO<sub>2</sub>. A broad signal in the excitonic PL spectra from 350 to 500 nm can be observed in these samples, resulting from the transition of excitons, such as photoinduced electrons trapped by oxygen vacancies and defects and the recombination of photo-induced electrons and holes. It can be observed that the PL intensity of N-TiO<sub>2</sub> and Au/N-TiO<sub>2</sub> are higher than that of TiO<sub>2</sub> and Au/TiO<sub>2</sub>, respectively, which can be attributed to the implanted N species. It was reported that the localized N doping level, oxygen vacancies, and other defect states, such as the Ti 3d state, can trap photogenerated electrons, thus inducing a high recombination rate [41]. The PL intensities

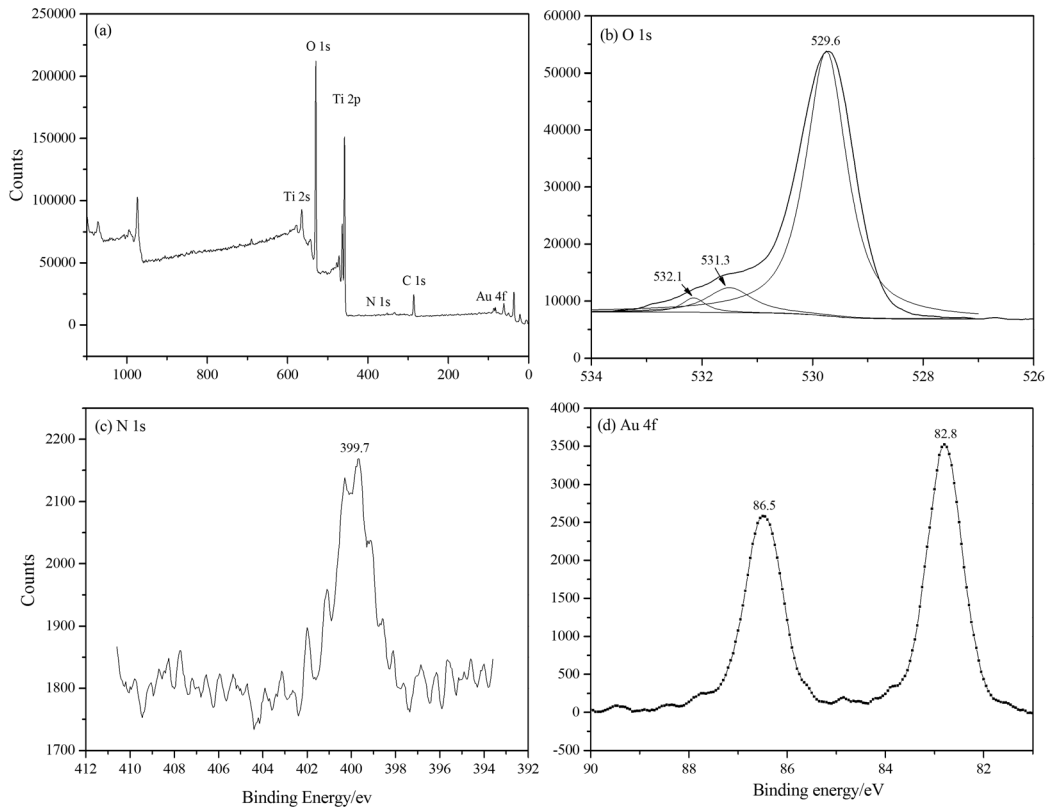


**Figure 3. XPS spectra of (a) Au/N-TiO<sub>2</sub> and core level spectra of (b) O 1s, (c) N 1s, and (d) Au 4f.**  
doi:10.1371/journal.pone.0103671.g003

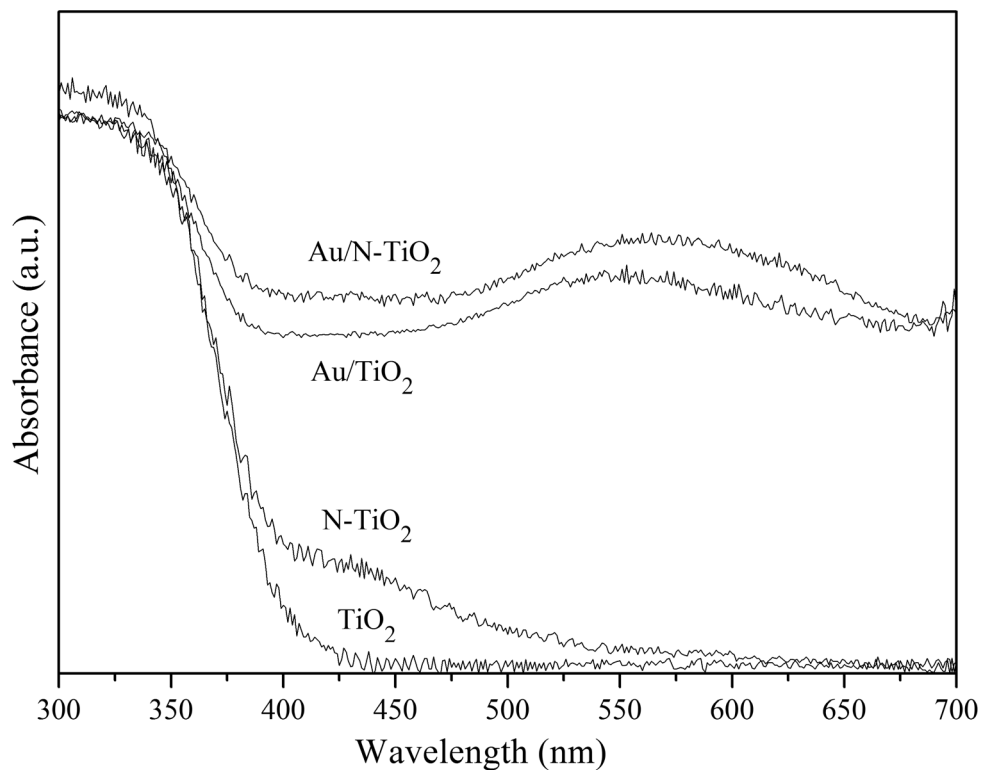


**Figure 4. UV-vis diffuse reflectance spectra of TiO<sub>2</sub>, Au/TiO<sub>2</sub>, N-TiO<sub>2</sub>, and Au/N-TiO<sub>2</sub>.**  
doi:10.1371/journal.pone.0103671.g004

of the Au-loaded samples (Au/TiO<sub>2</sub> and Au/N-TiO<sub>2</sub>) are much lower than those of the samples without Au (TiO<sub>2</sub> and N-TiO<sub>2</sub>), implying a lower recombination rate for the electrons and holes, which is mainly dependent on the formation of a Schottky barrier at the interface between Au/TiO<sub>2</sub> and Au/N-TiO<sub>2</sub>; this barrier can rapidly enhance the transfer of photo-induced electrons and simultaneously retard the recombination of electrons and holes [42]. The Fermi level of Au is lower than that of TiO<sub>2</sub>. When these two materials are electrically connected, photogenerated electrons in TiO<sub>2</sub> can readily be transferred to the Au nanoparticles and form a new quasi-Fermi level ( $E'_F$ ) [43].

### Photocatalytic activity

The H<sub>2</sub> evolution from photocatalytic water splitting reaction under irradiation of UV and UV-vis light was used to evaluate the photocatalytic performance of TiO<sub>2</sub>, N-TiO<sub>2</sub>, Au/TiO<sub>2</sub>, and Au/N-TiO<sub>2</sub>, as shown in Figure 6. Under the irradiation of UV light (Figure 6a), the N-TiO<sub>2</sub> and Au/N-TiO<sub>2</sub> samples show lower H<sub>2</sub> evolution rates than their corresponding samples without nitrogen doping (0.69 and 1.75  $\mu\text{mol}\cdot\text{h}^{-1}$  for N-TiO<sub>2</sub> and TiO<sub>2</sub>, respectively; 26.17 and 29.00  $\mu\text{mol}\cdot\text{h}^{-1}$  for Au/N-TiO<sub>2</sub> and Au/TiO<sub>2</sub>, respectively), confirming that the N doping has an acceleration on photogenerated electrons and holes recombination. After Au loading on pure TiO<sub>2</sub> and N-TiO<sub>2</sub>, the H<sub>2</sub> production are greatly enhanced due to the effective segregation of photo-induced electrons and holes resulting from the Schottky barrier at the interface of Au/TiO<sub>2</sub> and Au/N-TiO<sub>2</sub> [44], which is consistent with the result of PL. Under the irradiation of UV-vis light (Figure 6b), however, the N-TiO<sub>2</sub> and Au/N-TiO<sub>2</sub> samples show higher H<sub>2</sub> evolution rates than their corresponding nitrogen-free samples (TiO<sub>2</sub> and Au/TiO<sub>2</sub>). The H<sub>2</sub> evolution rates increase from 7.65 (TiO<sub>2</sub>) and 321.35 (Au/TiO<sub>2</sub>)  $\mu\text{mol}\cdot\text{h}^{-1}$  to 21.56 (N-

TiO<sub>2</sub>) and 412.60 (Au/N-TiO<sub>2</sub>)  $\mu\text{mol}\cdot\text{h}^{-1}$ , respectively. For N-TiO<sub>2</sub>, the enhancement of photocatalytic activity can be attributed to the doping of N, which can induce a visible light response in the TiO<sub>2</sub> original photocatalyst. The Au/N-TiO<sub>2</sub> sample has the highest UV-vis light hydrogen evolution rate because both the N doping and the SPR effect from the Au particles can induce a visible light response. That is, the cooperative effect of the N dopant and the Au particles results in an enhancement of the visible light photocatalytic activity for H<sub>2</sub> evolution, thereby greatly enhancing the utilization of sunlight.

The repeated hydrogen evolution tests over Au/N-TiO<sub>2</sub> under UV-vis light in pure water and in methanol/water solution were performed by purging of Ar in every 8 h. Fig 7a shows that the photocatalyst is able to split water for hydrogen evolution without adding methanol and the stability of this photocatalyst is good. This, in turn, indicates that methanol can greatly enhance the hydrogen production rate as a sacrificial agent. The stability of Au/N-TiO<sub>2</sub> photocatalyst in methanol/water solution is shown in Fig 7b, and as the increase of recycling times, the photocatalytic activity decrease slightly probably due to the loss of methanol in every recycling experiment.

### Photoelectrochemical characterizations

To further investigate the photoelectric properties of the as-prepared samples, photoelectrochemical measurements were performed. The transient photocurrents of TiO<sub>2</sub>, N-TiO<sub>2</sub>, Au/TiO<sub>2</sub>, and Au/N-TiO<sub>2</sub> under the irradiation of UV and visible light for 20 s are shown in Figure 8. Under the illumination of UV light (Figure 8a), the photocurrent responses of as-prepared samples follow the order TiO<sub>2</sub> > Au/TiO<sub>2</sub> > Au/N-TiO<sub>2</sub> > N-TiO<sub>2</sub>. While the currents of photocatalytic activity are as follows: Au/TiO<sub>2</sub> > Au/N-TiO<sub>2</sub> > TiO<sub>2</sub> > N-TiO<sub>2</sub>. This small

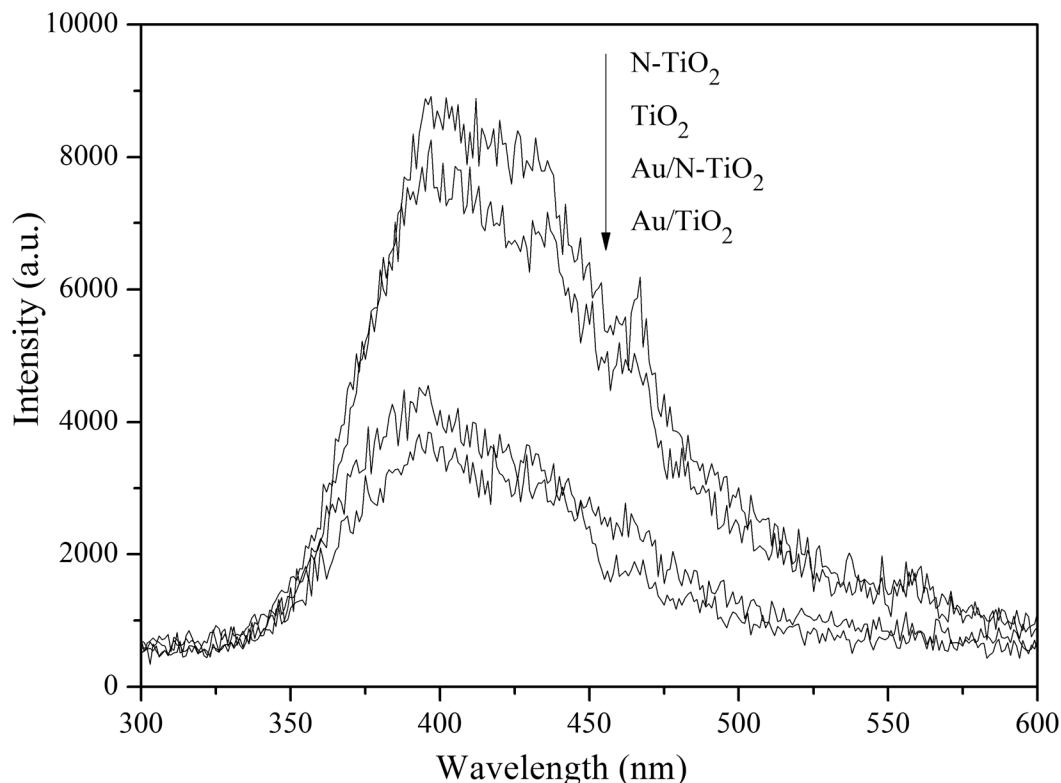


**Figure 5.** PL emission spectra of TiO<sub>2</sub>, Au/TiO<sub>2</sub>, N-TiO<sub>2</sub>, and Au/N-TiO<sub>2</sub> under the irradiation of 254 nm.

doi:10.1371/journal.pone.0103671.g005

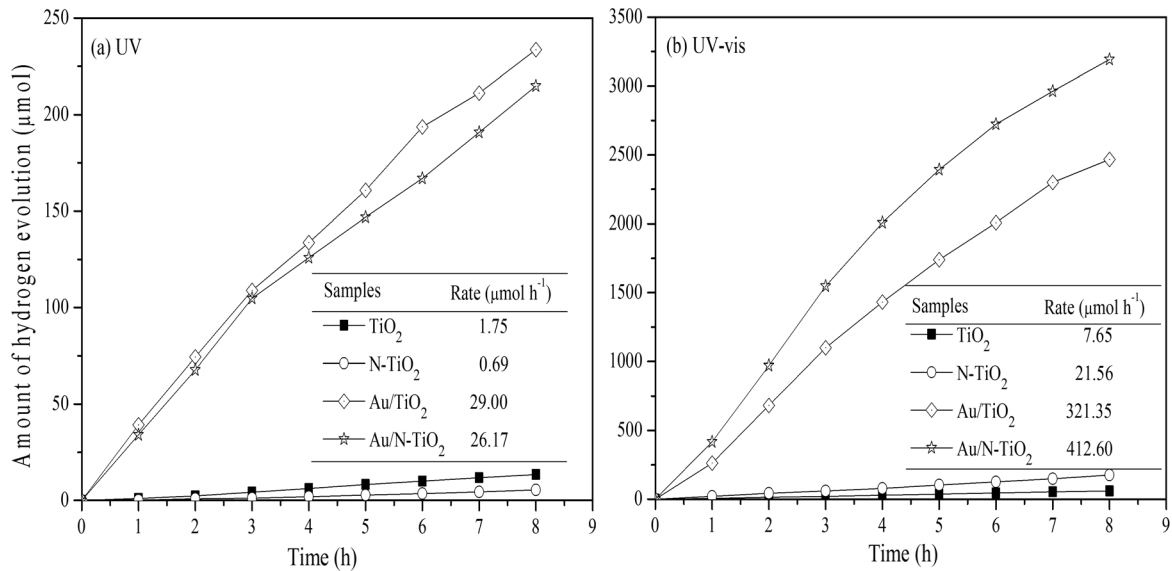


**Figure 6. Photocatalytic activity for water splitting under the irradiation of (a) UV and (b) UV-vis light.**  
doi:10.1371/journal.pone.0103671.g006

inconsistency can be attributed to two aspects: 1) the deposited gold nanoparticles decrease the number of photons reaching the TiO<sub>2</sub> and N-TiO<sub>2</sub> surface and reduce the surface area in contact with the electrolytes [37] and 2) electrons hopping across the particle boundaries are trapped on the surfaces of the Au/TiO<sub>2</sub> and Au/N-TiO<sub>2</sub> electrodes, decreasing the efficiency of the photocurrent collection at the ITO base [45]. Under visible light irradiation (Figure 8b), TiO<sub>2</sub> shows a lower photocurrent than N-TiO<sub>2</sub>, Au/TiO<sub>2</sub>, or Au/N-TiO<sub>2</sub>. For N-TiO<sub>2</sub>, the photocurrent response is attributed to the extension of the photonic absorption due to N doping. For Au/TiO<sub>2</sub>, the measured photocurrent result proves the SPR effect due to the modified Au particles. The highest photocurrent response from Au/N-TiO<sub>2</sub> suggests cooperation between the visible light response of the N dopant and the

SPR effect of the Au particles, which is consistent with the results in the Photocatalytic Activity section.

EIS for Au/N-TiO<sub>2</sub> was obtained to further investigate the cooperation between N doping and Au loading on the charge separation efficiency under visible light irradiation (Figure 9). The Nyquist plots show a pronounced semicircle at the high frequencies and a straight sloping line at low frequencies in both the dark and the irradiated cases. The diameters of the semicircles correspond to the charge-transfer resistance at the electrode interface, whereas the straight sloping line is related to the diffusion process of the reactive species [46]. The inset in Figure 9 is the proposed equivalent circuit and the fitting results for Au/N-TiO<sub>2</sub>. R<sub>s</sub> is the electrolyte resistance and also includes the contact and charge transfer resistances at the counter electrode/electrolyte

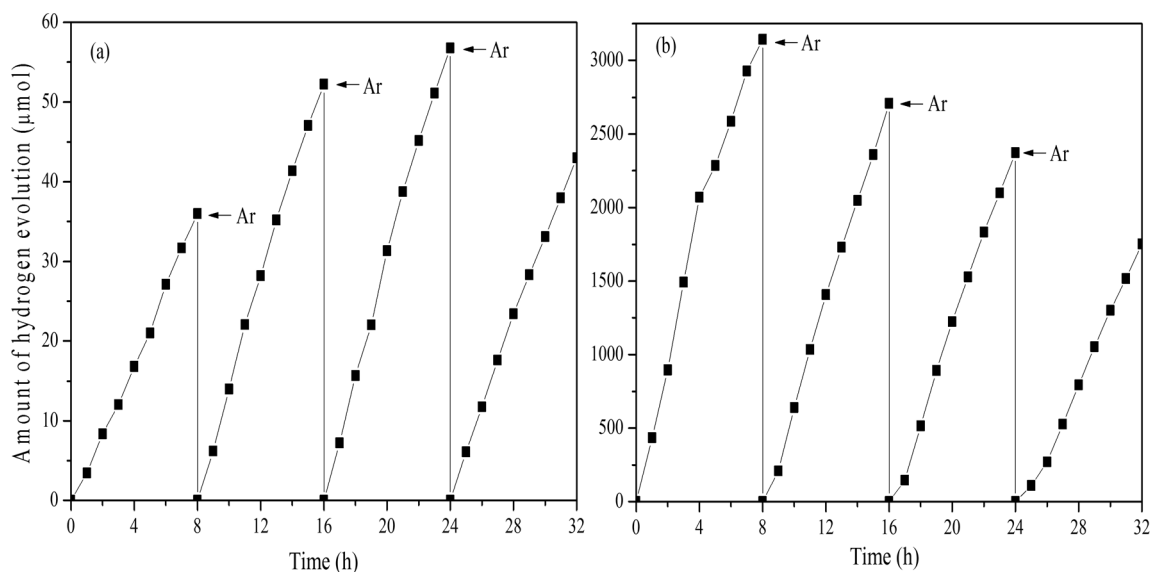


**Figure 7. The repeated hydrogen evolution tests over Au/N-TiO<sub>2</sub> under UV-vis light in (a) pure water and (b) methanol/water solution with purging of Ar in every 8 h.**  
doi:10.1371/journal.pone.0103671.g007

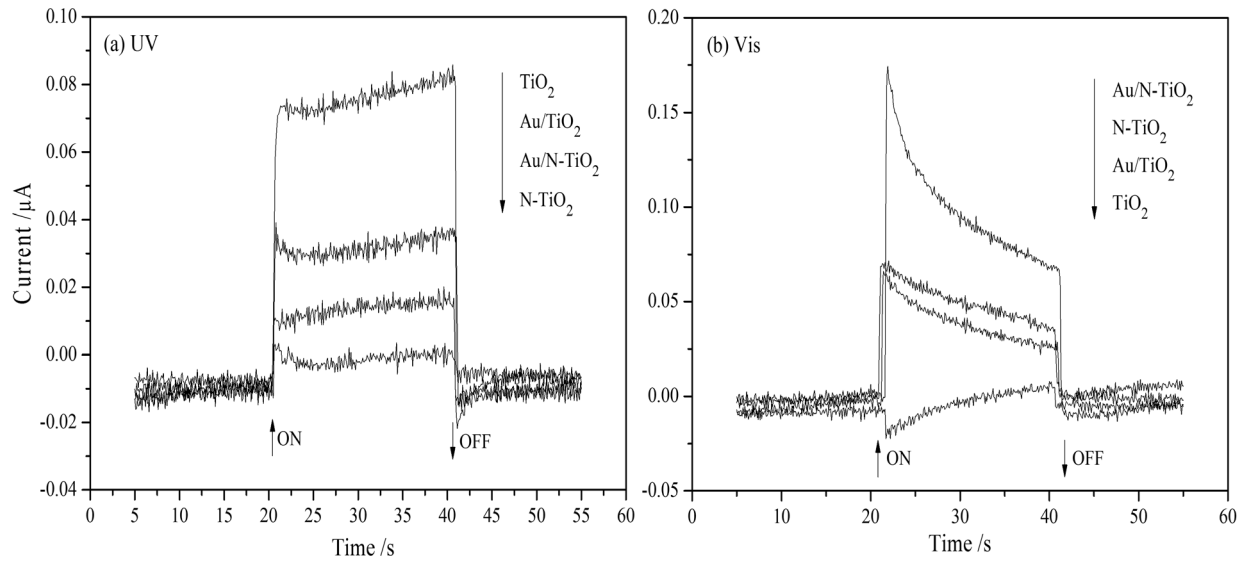


**Figure 8. Photocurrents of TiO<sub>2</sub>, N-TiO<sub>2</sub>, Au/TiO<sub>2</sub>, and Au/N-TiO<sub>2</sub> electrodes at zero bias voltage irradiated with (a) UV ( $\lambda=254$  nm) and (b) visible light ( $\lambda>400$  nm) for 20 s.**

doi:10.1371/journal.pone.0103671.g008

[47].  $R_{ct}$  is the electron-transfer resistance. CPE is the constant phase element, which also represents the double layer capacitance.  $W_s$  is the Warburg impedance, which is related to the diffusion of the reactive species at the surface of the electrodes and is illustrated by the straight line in the Nyquist plots. The contribution of the

visible light response for doped N and loaded Au is identified by the decreasing of  $R_{ct}$  and the increasing of double layer capacitance under illumination because TiO<sub>2</sub> is not photoactive under visible light. As observed, the value of  $R_{ct}$  for the Au/N-TiO<sub>2</sub> electrode decreases from 185  $\Omega \cdot \text{cm}^{-2}$  in the dark to 146

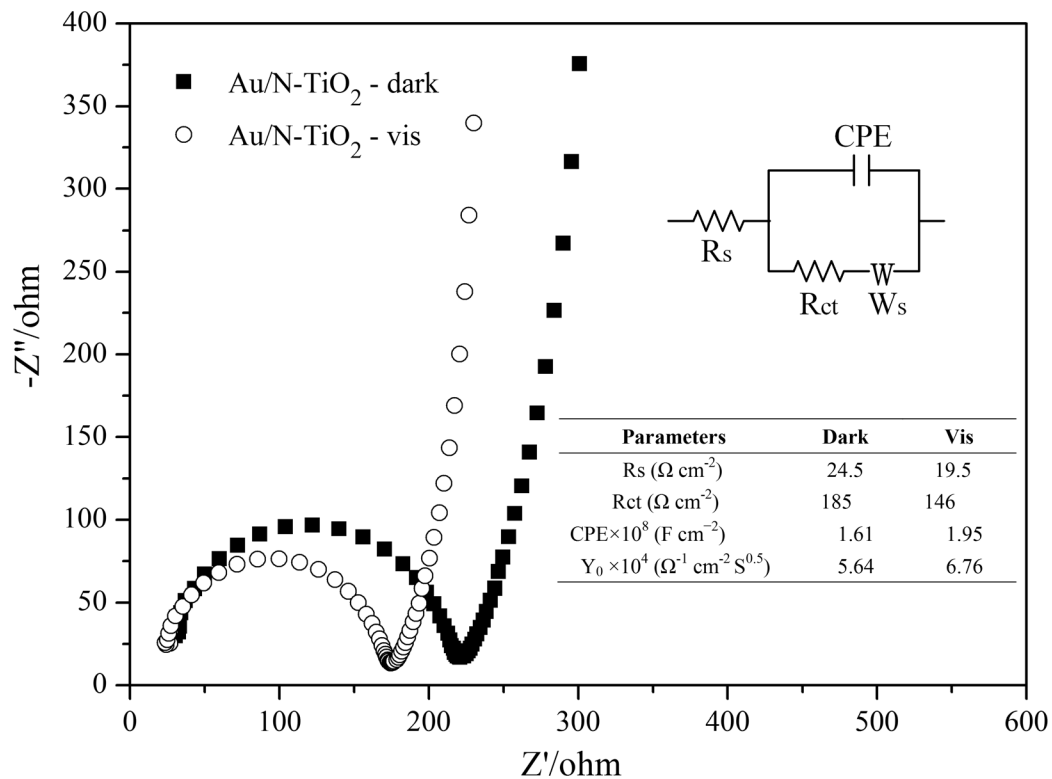


**Figure 9. EIS Nyquist plots for Au/N-TiO<sub>2</sub> in dark and under the irradiation of visible light.** Inset is the suggested equivalent circuit and the fitting results for Au/N-TiO<sub>2</sub>.  $R_s$  and  $R_{ct}$  are the electrolyte and electron-transfer resistance, respectively. CPE is the constant phase element, which also represents the double layer capacitance.  $W_s$  is the Warburg impedance.  $Y_0$  is the value of admittance and expresses a reciprocal relationship to the Warburg coefficient, which is able to predict the Warburg impedance and diffusion coefficient.

doi:10.1371/journal.pone.0103671.g009



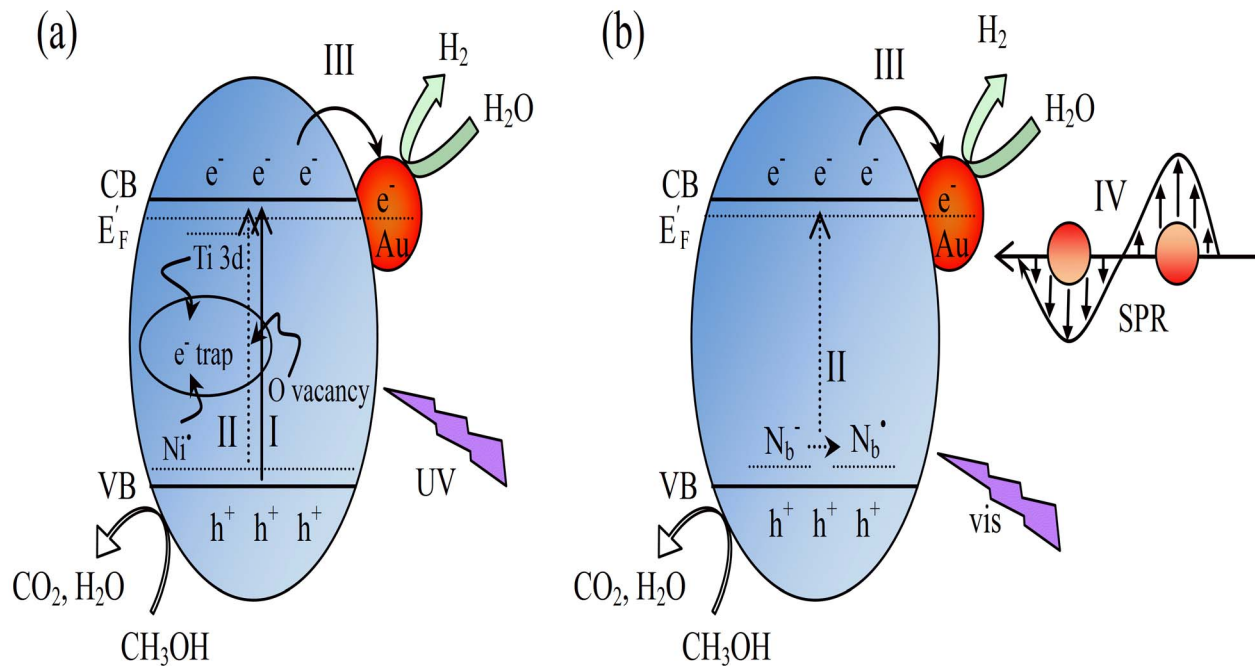


**Figure 10. Schematic illustration of Au/N-TiO<sub>2</sub> for water splitting under the irradiation of (a) UV and (b) visible light.** Pathway I denotes the generation of charge carriers in TiO<sub>2</sub>. Pathway II represents the reversible electron transfer between charged diamagnetic N<sub>b</sub><sup>-</sup> and neutral paramagnetic N<sub>b</sub><sup>•</sup>, and the excitation of electrons into the conduction band. Pathway III shows the acceleration of photo-induced electrons transfer by Au loading. Pathway IV denotes the SPR effect of loaded Au nanoparticles.  
doi:10.1371/journal.pone.0103671.g010

$\Omega \cdot \text{cm}^{-2}$  under visible light illumination, while the value of CPE increases from  $1.61 \times 10^{-8} \text{ F} \cdot \text{cm}^{-2}$  in the dark to  $1.95 \times 10^{-8} \text{ F} \cdot \text{cm}^{-2}$  under visible light illumination, manifesting as a faster charge transfer under visible light illumination due to the N doping and Au loading [48].

Figure 10 depicts sketches of the main charge-transfer process of Au/N-TiO<sub>2</sub> for water splitting. Under UV irradiation (Figure 10a), charges are mainly generated in the TiO<sub>2</sub>. The N dopant, oxygen vacancies and Ti 3d state can trap photogenerated electrons, delaying the separation of the electrons and holes. The Schottky barrier at the Au/N-TiO<sub>2</sub> interface can rapidly enhance the transfer of photoinduced electrons to Au nanoparticles and boost the photocatalytic activity for hydrogen production. Under visible light irradiation (Figure 10b), both the implanted N and the loaded Au contribute to the generation of electrons. Diamagnetic N<sub>b</sub><sup>-</sup> can transform into neutral paramagnetic N<sub>b</sub><sup>•</sup> and simultaneously excite electrons from the N states into the conduction band. The strong local electromagnetic field will increase the electron-hole pair generation rate in Au and enhance the visible light photocatalytic activity accordingly. The Au nanoparticles also play an important role in increasing the transfer of electrons under visible light irradiation.

## Conclusions

Au/N-TiO<sub>2</sub> photocatalyst was prepared via hydrothermal synthesis and ammonia impregnation and followed by a typical photoreduction method. XRD characterization described the change in the crystal structure from P25 to Au/N-TiO<sub>2</sub>. TEM and

XPS indicated that metallic Au can be loaded as Au<sup>0</sup> on the surface of the N-TiO<sub>2</sub> photocatalyst, and the nitrogen species were in the form of interstitial nitrogen. The results from the DRS, PL, and photoelectrochemical characterization indicated an extension of the light absorption into the visible region after Au loading and N doping, and the electron-hole recombination rate was effectively inhibited by the Au particles. Under UV light irradiation, the N-TiO<sub>2</sub> and Au/N-TiO<sub>2</sub> samples showed lower H<sub>2</sub> evolution than the corresponding samples without nitrogen (TiO<sub>2</sub> and Au/TiO<sub>2</sub>). Under UV-vis light irradiation, the N-TiO<sub>2</sub> and Au/N-TiO<sub>2</sub> samples showed more H<sub>2</sub> evolution than the corresponding nitrogen-free samples (TiO<sub>2</sub> and Au/TiO<sub>2</sub>). This finding indicated a synergic effect between the doped N and the Au in the enhancement of the visible light photocatalytic activity for H<sub>2</sub> evolution. Through N doping and Au loading, the as-prepared photocatalysts successfully increased the utilization of sunlight and enhanced the photocatalytic activity for H<sub>2</sub> evolution.

## Supporting Information

**File S1**  
(DOCX)

## Author Contributions

Conceived and designed the experiments: WRZ ZYA JSD. Performed the experiments: WRZ ZYA JSD. Analyzed the data: WRZ ZYA JSD MZ. Contributed reagents/materials/analysis tools: WRZ ZYA JSD. Contributed to the writing of the manuscript: WRZ ZYA MZ.

## References

- Jia T, Kolpin A, Ma C, Chan RCT, Kwok WM, et al. (2014) A graphene dispersed CdS-MoS<sub>2</sub> nanocrystal ensemble for cooperative photocatalytic hydrogen production from water. *Chem Commun* 50: 1185–1188.
- Yang G, Yan W, Zhang Q, Shen S, Ding S (2013) One-dimensional CdS/ZnO core/shell nanofibers via single-spinneret electrospinning: tunable morphology and efficient photocatalytic hydrogen production. *Nanoscale* 5: 12432–12439.

3. Wang D, Hisatomi T, Takata T, Pan C, Katayama M, et al. (2013) Core/shell photocatalyst with spatially separated co-catalysts for efficient reduction and oxidation of water. *Angew Chem Int Edit* 52: 11252–11256.
4. Zheng Z, Zhao J, Yuan Y, Liu H, Yang D, et al. (2013) Tuning the surface structure of nitrogen-doped TiO<sub>2</sub> nanofibres—an effective method to enhance photocatalytic activities of visible-light-driven green synthesis and degradation. *Chem-Eur J* 19: 5731–5741.
5. Xiang Q, Yu J, Wang W, Jaroniec M (2011) Nitrogen self-doped nanosized TiO<sub>2</sub> sheets with exposed {001} facets for enhanced visible-light photocatalytic activity. *Chem Commun* 47: 6906–6908.
6. Lin Z, Orlov A, Lambert RM, Payne MC (2005) New insights into the origin of visible light photocatalytic activity of nitrogen-doped and oxygen-deficient anatase TiO<sub>2</sub>. *J Phys Chem B* 109: 20948–20952.
7. Zhang J, Wu Y, Xing M, Leghari SAK, Sajjad S (2010) Development of modified N doped TiO<sub>2</sub> photocatalyst with metals, nonmetals and metal oxides. *Energ Environ Sci* 3: 715–726.
8. Wang J, Tafen DN, Lewis JP, Hong Z, Manivannan A, et al. (2009) Origin of photocatalytic activity of nitrogen-doped TiO<sub>2</sub> nanobelts. *J Am Chem Soc* 131: 12290–12297.
9. Taboada E, Angurell I, Llorca J (2014) Dynamic photocatalytic hydrogen production from ethanol-water mixtures in an optical fiber honeycomb reactor loaded with Au/TiO<sub>2</sub>. *J Catal* 309: 460–467.
10. Kominami H, Yamamoto S, Imamura K, Tanaka A, Hashimoto K (2014) Photocatalytic chemoselective reduction of epoxides to alkenes along with formation of ketones in alcoholic suspensions of silver-loaded titanium (iv) oxide at room temperature without the use of reducing gases. *Chem Commun* 50: 4558–4560.
11. Ohno T, Higo T, Murakami N, Saito H, Zhang Q, et al. (2014) Photocatalytic reduction of CO<sub>2</sub> over exposed-crystal-face-controlled TiO<sub>2</sub> nanorod having a brookite phase with co-catalyst loading. *Appl Catal B-Environ* 152: 309–316.
12. Wang P, Huang B, Zhang X, Qin X, Dai Y, et al. (2011) Highly efficient visible light plasmonic photocatalysts Ag@Ag (Cl, Br) and Ag@AgCl-AgI. *Chem-CatChem* 3: 360–364.
13. Zhou X, Liu G, Yu J, Fan W (2012) Surface plasmon resonance-mediated photocatalysis by noble metal-based composites under visible light. *J Mater Chem* 22: 21337–21354.
14. Seh ZW, Liu S, Low M, Zhang SY, Liu Z, et al. (2012) Janus Au-TiO<sub>2</sub> photocatalysts with strong localization of plasmonic near-fields for efficient visible-light hydrogen generation. *Adv Mater* 24: 2310–2314.
15. Li P, Wei Z, Wu T, Peng Q, Li Y (2011) Au-ZnO hybrid nanopyramids and their photocatalytic properties. *J Am Chem Soc* 133: 5660–5663.
16. Graciani J, Nambu A, Evans J, Rodriguez JA, Sanz JF (2008) Au $\leftrightarrow$ N synergy and N-doping of metal oxide-based photocatalysts. *J Am Chem Soc* 130: 12056–12063.
17. Tian B, Li C, Gu F, Jiang H (2009) Synergetic effects of nitrogen doping and Au loading on enhancing the visible-light photocatalytic activity of nano-TiO<sub>2</sub>. *Catal Commun* 10: 925–929.
18. Wu Y, Liu H, Zhang J, Chen F (2009) Enhanced photocatalytic activity of nitrogen-doped titania deposited with gold. *J Phys Chem C* 113: 14689–14695.
19. Dong F, Zhao W, Wu Z (2008) Characterization and photocatalytic activities of C, N and S co-doped TiO<sub>2</sub> with 1D nanostructure prepared by the nanoconfinement effect. *Nanotechnology* 19: 365607.
20. Iliev V, Tomova D, Todorovska R, Oliver D, Petrov L, et al. (2006) Photocatalytic properties of TiO<sub>2</sub> modified with gold nanoparticles in the degradation of oxalic acid in aqueous solution. *Appl Catal A-Gen* 313: 115–121.
21. Zhao W, Zhang J, Zhu X, Zhang M, Tang J, et al. (2013) Enhanced nitrogen photofixation on Fe-doped TiO<sub>2</sub> with highly exposed (101) facets in the presence of ethanol as scavenger. *Appl Catal B-Environ* 144: 468–477.
22. Mao Y, Wong SS (2006) Size- and shape-dependent transformation of nanosized titanate into analogous anatase titania nanostructures. *J Am Chem Soc* 128: 8217–8226.
23. Erdem B, Hunsicker RA, Simmons GW, Sudol ED, Dimonie VL, et al. (2001) XPS and FTIR surface characterization of TiO<sub>2</sub> particles used in polymer encapsulation. *Langmuir* 17: 2664–2669.
24. Wu D, Long M, Cai W, Chen C, Wu Y (2010) Low temperature hydrothermal synthesis of N-doped TiO<sub>2</sub> photocatalyst with high visible-light activity. *J Alloy Compd* 502: 289–294.
25. Sreethawong T, Laechalee S, Chavadej S (2009) Use of Pt/N-doped mesoporous-assembled nanocrystalline TiO<sub>2</sub> for photocatalytic H<sub>2</sub> production under visible light irradiation. *Catal Commun* 10: 538–543.
26. Di Valentin C, Finazzi E, Pacchioni G, Selloni A, Livraghi S, et al. (2007) N-doped TiO<sub>2</sub>: theory and experiment. *Chem Phys* 339: 44–56.
27. Jiang Z, Yang F, Luo N, Chu BT, Sun D, et al. (2008) Solvothermal synthesis of N-doped TiO<sub>2</sub> nanotubes for visible-light-responsive photocatalysis. *Chem Commun*: 6372–6374.
28. Wang J, Zhu W, Zhang Y, Liu S (2007) An efficient two-step technique for nitrogen-doped titanium dioxide synthesizing: visible-light-induced photodecomposition of methylene blue. *J Phys Chem C* 111: 1010–1014.
29. Li X, Fan T, Zhou H, Zhu B, Ding J, et al. (2008) A facile way to synthesize biomorphic N-TiO<sub>2</sub> incorporated with Au nanoparticles with narrow size distribution and high stability. *Micropor Mesopor Mat* 116: 478–484.
30. Chen JJ, Wu JCS, Wu PC, Tsai DP (2011) Plasmonic photocatalyst for H<sub>2</sub> evolution in photocatalytic water splitting. *J Phys Chem C* 115: 210–216.
31. Epling WS, Hoefflund GB, Weaver JF, Tsubota S, Haruta M (1996) Surface characterization study of Au/ $\alpha$ -Fe<sub>2</sub>O<sub>3</sub> and Au/Co<sub>3</sub>O<sub>4</sub> low-temperature CO oxidation catalysts. *J Phys Chem C* 100: 9929–9934.
32. Di Valentin C, Pacchioni G, Selloni A (2004) Origin of the different photoactivity of N-doped anatase and rutile TiO<sub>2</sub>. *Phys Rev B* 70: 085116.
33. Livraghi S, Paganini MC, Giamello E, Selloni A, Di Valentin C, et al. (2006) Origin of photoactivity of nitrogen-doped titanium dioxide under visible light. *J Am Chem Soc* 128: 15666–15671.
34. Tanaka A, Ogino A, Iwaki M, Hashimoto K, Ohnuma A, et al. (2012) Gold-titanium (iv) oxide plasmonic photocatalysts prepared by a colloid-photodeposition method: correlation between physical properties and photocatalytic activities. *Langmuir* 28: 13105–13111.
35. DeSario PA, Pietron JJ, DeVantier DE, Brintlinger TH, Stroud RM, et al. (2013) Plasmonic enhancement of visible-light water splitting with Au-TiO<sub>2</sub> composite aerogels. *Nanoscale* 5: 8073–8083.
36. Garcia M (2011) Surface plasmons in metallic nanoparticles: fundamentals and applications. *J Phys D Appl Phys* 44: 283001.
37. Liu Z, Hou W, Pavaskar P, Aykol M, Cronin SB (2011) Plasmon resonant enhancement of photocatalytic water splitting under visible illumination. *Nano Lett* 11: 1111–1116.
38. Wang P, Huang B, Dai Y, Whangbo MH (2012) Plasmonic photocatalysts: harvesting visible light with noble metal nanoparticles. *Phys Chem Chem Phys* 14: 9813–9825.
39. Yu JG, Yu HG, Cheng B, Zhao XJ, Yu JC, et al. (2003) The effect of calcination temperature on the surface microstructure and photocatalytic activity of TiO<sub>2</sub> thin films prepared by liquid phase deposition. *J Phys Chem B* 107: 13871–13879.
40. Cong Y, Zhang J, Chen F, Anpo M (2007) Synthesis and characterization of nitrogen-doped TiO<sub>2</sub> nanophotocatalyst with high visible light activity. *J Phys Chem C* 111: 6976–6982.
41. Hoang S, Guo S, Hahn NT, Bard AJ, Mullins CB (2011) Visible light driven photoelectrochemical water oxidation on nitrogen-modified TiO<sub>2</sub> nanowires. *Nano Lett* 12: 26–32.
42. Tian B, Li C, Gu F, Jiang H (2009) Synergetic effects of nitrogen doping and Au loading on enhancing the visible-light photocatalytic activity of nano-TiO<sub>2</sub>. *Catal Commun* 10: 925–929.
43. Zhang J, Wang Y, Zhang J, Lin Z, Huang F, et al. (2013) Enhanced photocatalytic hydrogen production activities of Au-loaded ZnS flowers. *ACS Appl Mater Inter* 5: 1031–1037.
44. Zhang P, Shao C, Li X, Zhang M, Zhang X, et al. (2012) In situ assembly of well-dispersed Au nanoparticles on TiO<sub>2</sub>/ZnO nanofibers: a three-way synergistic heterostructure with enhanced photocatalytic activity. *J Hazard Mater* 237: 331–338.
45. Min Y, He G, Li R, Zhao W, Chen Y, et al. (2013) Doping nitrogen anion enhanced photocatalytic activity on TiO<sub>2</sub> hybridized with graphene composite under solar light. *Sep Purif Technol* 106: 97–104.
46. Wang H, Zhang C, Liu Z, Wang L, Han P, et al. (2011) Nitrogen-doped graphene nanosheets with excellent lithium storage properties. *J Mater Chem* 21: 5430–5434.
47. Bessekhouad Y, Brahim R, Hamdini F, Trari M (2012) Cu<sub>2</sub>S/TiO<sub>2</sub> heterojunction applied to visible light Orange II degradation. *J Photoch Photobio A* 248: 15–23.
48. Xin B, Ren Z, Hu H, Zhang X, Dong C, et al. (2005) Photocatalytic activity and interfacial carrier transfer of Ag-TiO<sub>2</sub> nanoparticle films. *Appl Surf Sci* 252: 2050–2055.